Smart Mater. Struct. **8** (1999) 729–740. Printed in the UK PII: S0964-1726(99)02639-7

# Shape control of a beam using piezoelectric actuators

**Brij N Agrawal and Kirk E Treanor**

Naval Postgraduate School, Spacecraft Research and Design Center, Monterey, CA 93943, USA

Received 22 May 1998, in final form 4 March 1999

**Abstract.** This paper presents the analytical and experimental results on optimal placement of piezoceramic actuators for shape control of beam structures. The objective is to determine the optimum piezoceramic actuator locations and voltages to minimize the error between the desired shape and the achieved shape. The analytical model for predicting beam deformation due to a piezoelectric actuator is based on the Euler–Bernoulli model. The cost function has fifth-order polynomials in the actuator locations and second-order polynomials in actuator voltages. This difference resulted in difficulty in simultaneous optimization of actuator locations and voltages. Using embedded Nader and Mead simplex algorithms to separately optimize actuator locations and voltages was found to produce reliable results, converging to the same optimum solution for a variety of initial conditions. Experimental results show that the analytical model provides a reasonable prediction of actuator performance at low input voltage, but does not account for the nonlinear behavior of the piezoceramic and effects of hysteresis.

## 1. Introduction

For a communications satellite designer, providing precision surfaces for antenna reflectors has been a challenging problem. Surface errors are introduced by manufacturing errors, thermal distortion in orbit, moisture, loose joints, material degradation and creep. These reflectors are made of graphite–epoxy structures because of requirements for low thermal distortion. Significant time and cost are spent during fabrication, analysis and ground tests to minimize and determine the surface errors. Even with this effort, several current spacecraft antennas have experienced degraded performance due to higher than predicted surface errors. Smart sensors and actuators with the ability to correct on-orbit surface errors have great potential for use in these microwave devices. Smart actuators can also provide a desired change in antenna beam shape due to change in coverage requirements. Therefore, smart structure technology has the potential of not only improving the performance of these structures, but also reduction in cost for analyses and ground tests.

A number of smart materials are available which may be used as sensors or actuators. These materials include piezoelectric polymers and ceramics, shape memory alloys, electrorheological fluids and optical fibers. While significant research effort has been devoted to the use of smart structures for active vibration suppression, considerably less attention has been focused on the use of smart structures for shape control. At the Spacecraft Research and Design Center (SRDC) at the Naval Postgraduate School active vibration control and shape control using smart materials is an active area of research. This paper presents recent analytical results of research work at SRDC on shape control using piezoelectric actuators. Although piezoelectric materials have relatively small dimensional change capability, they are more than adequate for certain applications, such as countering thermal distortion and manufacturing surface errors in microwave devices. The research work examined the application of piezoceramic actuators and sensors for the shape control of a beam, a common structural element for large deployable antenna structures.

## 2. Analytical model

The beam under consideration is shown in figure 1. It is a cantilever beam with piezoceramic actuators bonded at locations $x_i$ ($i = 1, 2, \ldots, n$).

To determine transverse deflection of the composite beam, i.e., beam plus piezoceramic actuator, Euler–Bernoulli beam theory is used instead of plate theory. Euler–Bernoulli beam theory assumes that the transverse component of normal stress is negligible in comparison to the axial component. Therefore, the relation between actuator strain and stress is given by the following equation

$$\sigma_1 = E_1 (\varepsilon_1 - d_{31}\phi_3) \tag{1}$$

where $\sigma_1$ is the actuator stress in direction 1 ($x$), $E_1$ the modulus of elasticity of the actuator in direction 1, $\varepsilon_1$ the strain of the actuator in direction 1, $d_{31}$ the lateral charge coefficient of the actuator with poling direction along direction 3, $\phi_3$ the electric field $= V/t_p$, $V$ the applied voltage and $t_p$ the actuator thickness.

Crawley and Anderson [1] compared two models of beam curvature due to induced strain actuation by

0964-1726/99/060729+12$30.00  

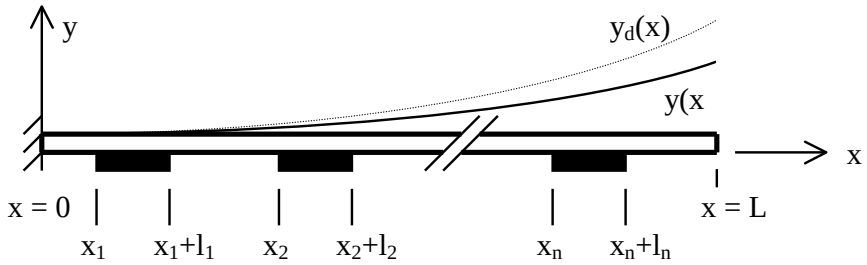


**Figure 1.** Beam with attached piezoceramic actuators.

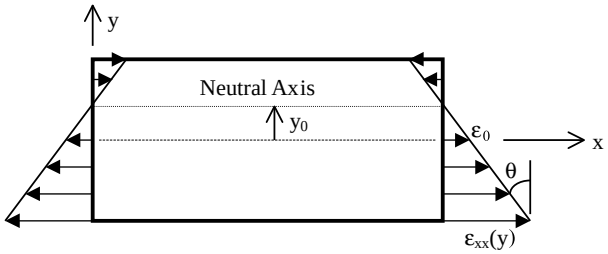


**Figure 2.** Linear strain distribution for Euler–Bernoulli beam.

piezoceramic actuators bonded to beam structures. The first model, initially presented by Crawley and de Luis [2], assumed uniform axial strain in a pair of piezoceramic actuators bonded symmetrically to the outer surface of a beam undergoing actuator-induced bending. The second model assumed that the beam behaves as an Euler–Bernoulli beam, with linear distribution of axial strain throughout the composite actuator beam cross-section as shown in figure 2. The predicted beam curvature under both models was compared to that predicted by a detailed two-dimensional finite element model. The Euler–Bernoulli model was found to provide results that are within 0.1% of the finite element model over the full range of possible actuator-to-beam thickness ratios, while the uniform strain model results diverged significantly for actuator thickness greater than 20% of the beam. The Euler–Bernoulli model was therefore judged to provide a much more accurate prediction of beam curvature produced by surface-bonded piezoceramic actuators.

As an example, for a beam with a symmetric piezoceramic actuator pair bonded to a section of a beam, as shown in figure 3, the axial strain at $y = 0$, $\varepsilon_0$, and curvature $\kappa$ about the $z$ axis are given by

$$\begin{aligned} \varepsilon_0 &= \frac{E_p d_{31} w_p\,(V_1 + V_2)}{(\mathrm{EA})_c} \\ \kappa &= \frac{E_p d_{31} w_p \left[\frac{t}{2} + t_b + \frac{t_p}{2}\right](V_1 - V_2)}{(\mathrm{EI})_c} \end{aligned} \tag{2}$$

where

$$(\mathrm{EA})_c = Ewt + 2E_b w_b t_b + 2E_p w_p t_p \tag{3}$$

$$\begin{aligned} (\mathrm{EI})_c = {} & \frac{Ewt^3}{12} + 2E_b w_b t_b \left[\left(\frac{t}{2}\right)^2 + \frac{t}{2}t_b + \frac{t_b^2}{3}\right] \\ & + 2E_p w_p t_p \left[\left(\frac{t}{2} + t_b\right)^2 + \left(\frac{t}{2} + t_b\right)t_p + \frac{t_p^2}{3}\right]. \end{aligned} \tag{4}$$

$w$, $w_b$, $w_p$ are the widths of the beam, bond and actuator, respectively; $E$, $E_b$, $E_p$ are the modulus of elasticity of the beam, bond and actuator, respectively; $t$, $t_b$, $t_p$ are the thickness of the beam, bond and actuator, respectively, and $V_1$ and $V_2$ are the input voltages to the actuators on the $+y$ side and $-y$ side of the beam, respectively.

For a beam with a single piezoceramic actuator bonded to a section of the beam, as shown in figure 4, the axial strain at $y = 0$ and the curvature of the composite beam are given by

$$\begin{aligned} \varepsilon_0 &= \frac{P_\Lambda\,(\mathrm{EI})_c - M_\Lambda\,(\mathrm{ES})_c}{(\mathrm{EA})_c\,(\mathrm{EI})_c - (\mathrm{ES})_c^2} \\ \kappa &= \frac{M_\Lambda}{(\mathrm{EI})_c} - \frac{(\mathrm{ES})_c}{(\mathrm{EI})_c}\left[\frac{P_\Lambda\,(\mathrm{EI})_c - M_\Lambda\,(\mathrm{ES})_c}{(\mathrm{EA})_c\,(\mathrm{EI})_c - (\mathrm{ES})_c^2}\right] \end{aligned} \tag{5}$$

where

$$(\mathrm{EA})_c = Ewt + E_b w_b t_b + E_p w_p t_p \tag{6}$$

$$(\mathrm{ES})_c = E_b w_b t_b\left(\frac{t}{2} + \frac{t_b}{2}\right) + E_p w_p t_p\left(\frac{t}{2} + t_b + \frac{t_p}{2}\right) \tag{7}$$

$$\begin{aligned} (\mathrm{EI})_c = {} & \frac{Ewt^3}{12} + E_b w_b t_b\left[\left(\frac{t}{2}\right)^2 + \frac{t}{2}t_b + \frac{t_b^2}{3}\right] \\ & + E_p w_p t_p\left[\left(\frac{t}{2} + t_b\right)^2 + \left(\frac{t}{2} + t_b\right)t_p + \frac{t_p^2}{3}\right] \end{aligned} \tag{8}$$

$$P_\Lambda = E_p d_{31} w_p V \tag{9}$$

$$M_\Lambda = E_p d_{31} w_p\left[\frac{t}{2} + t_b + \frac{t_p}{2}\right]V. \tag{10}$$

If the deformation of the beam is static and no external loads are applied, then the deformation of the beam is strictly a function of the actuator locations, lengths, actuator/beam curvatures per unit voltage and actuator input voltages. The beam curvature per unit voltage is given by

$$K_k = \frac{\kappa_k}{V_k} \qquad (k = 1,\ 2,\ \ldots,\ n)\,. \tag{11}$$

Using the previous equations, the transverse deflection $y(x)$ and slope $y'(x)$ for a beam with $n$ attached piezoceramic actuators are given by the following equations:

(a) For $x$ prior to the first actuator

$$\left.\begin{aligned} y'(x) &= 0 \\ y\,(x) &= 0 \end{aligned}\right\} \qquad (0 \leqslant x \leqslant x_1)\,. \tag{12}$$

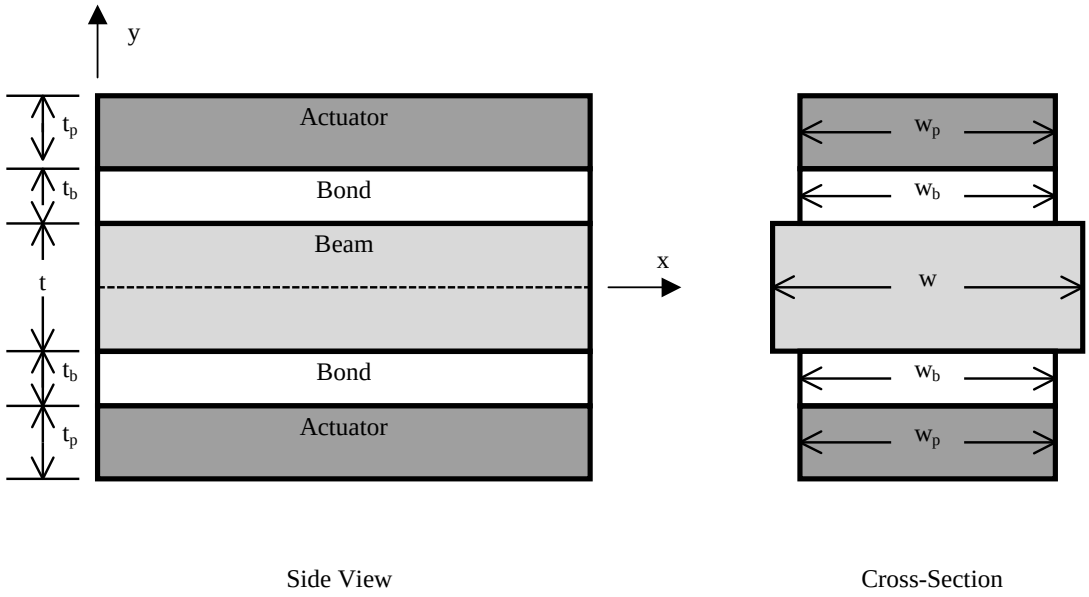


**Figure 3.** Schematic of stacked piezoceramic actuator pair bonded to beam.

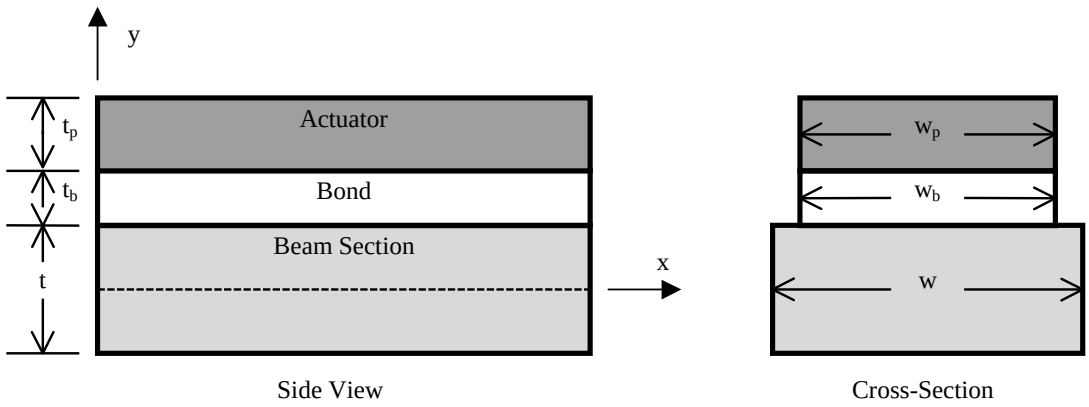


**Figure 4.** Schematic of single piezoceramic actuator bonded to beam.

(b) For $x$ on the first actuator

$$\left.\begin{array}{l} y'(x) = K_1 V_1 (x - x_1) \\ y(x) = \frac{K_1 V_1}{2} (x - x_1)^2 \end{array}\right\} \qquad (x_1 \leqslant x \leqslant x_1 + l_1)\,. \quad (13)$$

(c) For $x$ on actuator $k$

$$\left.\begin{array}{l} y'(x) = K_k V_k (x - x_k) + \sum\limits_{i=1}^{k-1} K_i V_i l_i \\ y(x) = \frac{K_k V_k}{2} (x - x_k)^2 + \sum\limits_{i=1}^{k-1} K_i V_i l_i \left(x - x_i - \frac{l_i}{2}\right) \end{array}\right\} \left(\begin{array}{l} x_k \leqslant x \leqslant x_k + l_k \\ k = 2, 3, ..., n \end{array}\right). \quad (14)$$

(d) For $x$ between actuator $k$ and $k + 1$

$$\left.\begin{array}{l} y'(x) = \sum\limits_{i=1}^{k} K_i V_i l_i \\ y(x) = \sum\limits_{i=1}^{k} K_i V_i l_i \left(x - x_i - \frac{l_i}{2}\right) \end{array}\right\} \left(\begin{array}{l} x_k + l_k \leqslant x \leqslant x_{k+1} \\ k = 1, 2, ..., n - 1 \end{array}\right). \quad (15)$$

(e) For $x$ between actuator $n$ and the free end of the beam

$$\left.\begin{array}{l} y'(x) = \sum\limits_{i=1}^{n} K_i V_i l_i \\ y(x) = \sum\limits_{i=1}^{n} K_i V_i l_i \left(x - x_i - \frac{l_i}{2}\right) \end{array}\right\} \quad (x_n + l_n \leqslant x \leqslant L) \quad (16)$$

(where $l_i$ is the length of the $i$th actuator).

## 3. Optimization

It is desired to determine the optimum location of piezoceramic actuators, and input voltages to achieve the desired beam shape. Optimization requires a suitable cost function to serve as a measure of performance for a given actuator configuration. The optimum actuator configuration achieves the absolute minimum value of the cost function among the set of all possible input variable values, including actuator position, length and input voltage.

An appropriate cost function for measuring actuator

performance in the static deflection of a cantilever beam is

$$J = \int_0^L [y(x) - y_d(x)]^2 \, \mathrm{d}x \tag{17}$$

where $x$ is the coordinate along the length of the beam and $y(x)$ and $y_d(x)$ are the actual and desired transverse beam deflections along the beam, respectively, as shown in figure 1.

The actuator locations and lengths are constrained by:

$$\begin{aligned} & x_1 \geqslant 0 \\ & x_i \geqslant x_{i-1} + l_{i-1} \qquad (i = 2, 3, \ldots, n) \\ & x_n + l_n \leqslant L \\ & l_i \geqslant 0 \qquad (i = 1, 2, \ldots, n)\,. \end{aligned} \tag{18}$$

Equations (18) ensure that all the actuators are located entirely on the beam without overlap and that all have nonnegative length. Furthermore, the input voltages to the piezoceramic actuators must lie within an operating range specified by:

$$V_{\min} \leqslant V_i \leqslant V_{\max} \qquad (i = 1, 2, \ldots, n) \tag{19}$$

where $V_{\min}$ and $V_{\max}$ are the actuator's minimum and maximum operating voltages and $V_i$ is the input voltage to the $i$th actuator.

The problem of optimizing equation (17) within the constraints of equations (18) and (19) can be expressed in Kuhn–Tucker (KT) form as: minimize equation (17) subject to:

$$\begin{aligned} g_1(\boldsymbol{z}) &= -x_1 \leqslant 0 \\ g_i(\boldsymbol{z}) &= x_{i-1} + l_{i-1} - x_i \leqslant 0 \qquad (i = 2, 3, \ldots, n) \\ g_{n+1}(\boldsymbol{z}) &= x_n + l_n - L \leqslant 0 \\ g_{n+1+i}(\boldsymbol{z}) &= -l_i \leqslant 0 \qquad (i = 1, 2, \ldots, n) \\ g_{2n+1+i}(\boldsymbol{z}) &= (V_i - V_{\min})(V_i - V_{\max}) \leqslant 0 \\ & \qquad (i = 1, 2, \ldots, n) \end{aligned} \tag{20}$$

where the vector of input variables, $\boldsymbol{z}$, is given by

$$\boldsymbol{z} = [x_1 \ldots x_n, l_1 \ldots l_n, V_1 \ldots V_n]^T\,. \tag{21}$$

The desired shape function $y_d(x)$ is selected to be a parabolic shape function given by:

$$y_d(x) = Cx^2. \tag{22}$$

The parabolic shape function is selected due to its applicability to common structures such as antenna reflectors. Substituting equations (22) and (12)–(16) into equation (17) gives an expression for the cost function:

$$\begin{aligned} J = {} & \frac{C^2 x_1^5}{5} \\ & + \sum_{k=1}^{n} \left\{ \begin{array}{l} (a_{2k} - C)^2 \, \frac{(x_k + l_k)^5 - x_k^5}{5} + 2(a_{2k} - C) a_{1k} \frac{(x_k + l_k)^4 - x_k^4}{4} \\ + \left[ 2(a_{2k} - C) a_{0k} + a_{1k}^2 \right] \frac{(x_k + l_k)^3 - x_k^3}{3} \\ + 2 a_{1k} a_{0k} \frac{(x_k + l_k)^2 - x_k^2}{2} + a_{0k}^2 l_k \end{array} \right\} \\ & + \sum_{k=1}^{n-1} \left\{ \begin{array}{l} C^2 \frac{x_{k+1}^5 - (x_k + l_k)^5}{5} - 2C b_{1k} \frac{x_{k+1}^4 - (x_k + l_k)^4}{4} \\ + \left( -2C b_{0k} + b_{1k}^2 \right) \frac{x_{k+1}^3 - (x_k + l_k)^3}{3} + 2 b_{1k} b_{0k} \frac{x_{k+1}^2 - (x_k + l_k)^2}{2} \\ + b_{0k}^2 (x_{k+1} - x_k - l_k) \end{array} \right\} \\ & + C^2 \frac{L^5 - (x_n + l_n)^5}{5} - 2C b_{1n} \frac{L^4 - (x_n + l_n)^4}{4} \\ & + \left( -2C b_{0n} + b_{1n}^2 \right) \frac{L^3 - (x_n + l_n)^3}{3} \\ & + 2 b_{1n} b_{0n} \frac{L^2 - (x_n + l_n)^2}{2} + b_{0n}^2 (L - x_n - l_n) \end{aligned} \tag{23}$$

where the coefficients $a_{ij}$ and $b_{ij}$ are obtained by rewriting the beam displacements in equations (12)–(16) as polynomials in $x$.

For $x$ prior to the first actuator:

$$y(x) = 0 \qquad (0 \leqslant x \leqslant x_1)\,. \tag{24}$$

For $x$ on actuator $k$:

$$y(x) = a_{2k} x^2 + a_{1k} x + a_{0k} \qquad \begin{pmatrix} x_k \leqslant x \leqslant x_k + l_k \\ k = 1, 2, \ldots, n \end{pmatrix}. \tag{25}$$

For $x$ between actuator $k$ and $k + 1$:

$$y(x) = b_{1k} x + b_{0k} \qquad \begin{pmatrix} x_k + l_k \leqslant x \leqslant x_{k+1} \\ k = 1, 2, \ldots, n-1 \end{pmatrix}. \tag{26}$$

For $x$ between actuator $n$ and the free end of the beam ($x = L$):

$$y(x) = b_{1n} x + b_{0n} \qquad (x_n + l_n \leqslant x \leqslant L) \tag{27}$$

where

$$\begin{aligned} a_{2k} &= \frac{K_k V_k}{2} \qquad (k = 1, 2, \ldots, n) \\ a_{1k} &= \begin{cases} -K_1 V_1 x_1 & (k = 1) \\ -K_k V_k x_k + \sum_{i=1}^{k-1} K_i V_i l_i & (k = 2, 3, \ldots, n) \end{cases} \\ a_{01} &= \begin{cases} \dfrac{K_1 V_1 x_1^2}{2} & (k = 1) \\ \dfrac{K_k V_k x_k^2}{2} - \sum_{i=1}^{k-1} K_i V_i l_i \left( x_i + \dfrac{l_i}{2} \right) & (k = 2, 3, \ldots, n) \end{cases} \\ b_{1k} &= \sum_{i=1}^{k} K_i V_i l_i \qquad (k = 1, 2, \ldots, n) \\ b_{0k} &= -\sum_{i=1}^{k} K_i V_i l_i \left( x_i + \frac{l_i}{2} \right) \qquad (k = 1, 2, \ldots, n). \end{aligned} \tag{28}$$

## 4. Algorithm for solution of optimization problem

The MATLAB software package was used for the development of an algorithm to optimize actuator placement and voltage for a given shape function and for fixed actuator and beam dimensions and properties. If the actuator dimensions and properties are fixed, then the lengths $l_i$ and curvatures per unit input voltage will be constant values.

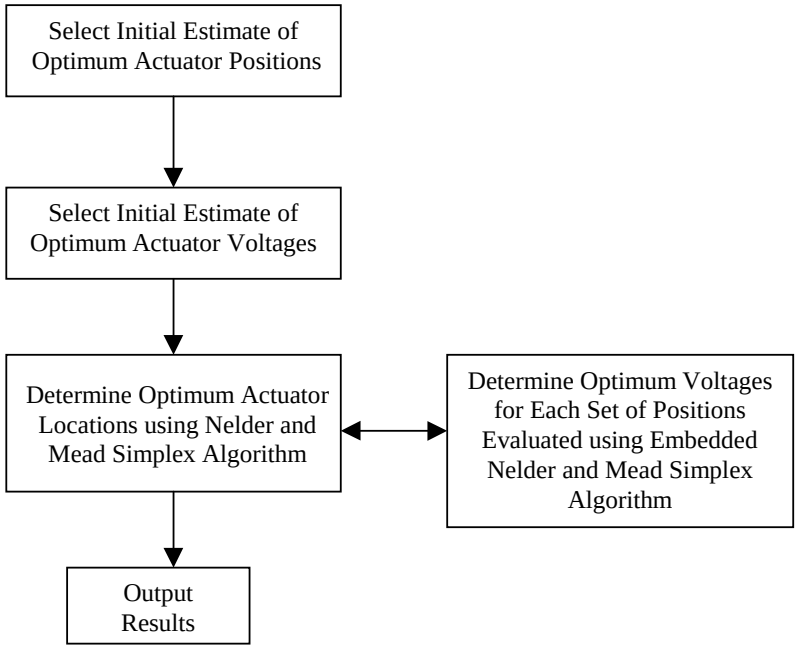


**Figure 5.** Actuator placement optimization algorithm.

The cost function is therefore minimized by optimizing the remaining variables $x_i$ and $V_i$.

The MATLAB Optimization Toolbox includes three functions intended for the optimization of multivariable functions. Two functions, *fminu* and *fmins*, perform unconstrained optimization of the input variables of a cost function, while one function, *constr*, performs optimization of the input variables subject to constraints on their values. *Fmins* uses the simplex search algorithm developed by Nelder and Mead. *Fminu* uses the quasi-Newton method of Broyden, Fletcher, Goldfrab and Shanno (BFGS), with a mixed quadratic and cubic line search procedure to determine a search direction at each iteration. *Constr* also uses a BFGS quasi-Newton method to solve a quadratic subproblem at each iteration of a sequential quadratic programming routine. Initial attempts to optimize actuator placement and voltage simultaneously using these algorithms proved unsuccessful. *Fmins* produced better results than *fminu* and *constr*, but not robust for all cases.

A revised approach to the optimization problem was developed, drawing on the work of Clark and Fuller [3] and Wang *et al* [4] to optimize actuator location for acoustic control. The latter group noted that the mathematical inconsistency in the order of the voltages and actuator locations in their objective function requires independent solutions for the voltages and locations. The same approach is applied for the present problem. First, given initial actuator voltages, determine the optimum locations of the actuators. Next for the calculated optimum actuator locations, determine the optimum actuator voltages. Next for the calculated optimum actuator voltages re-determine the optimum actuator locations. This process is repeated until we obtain a minimum cost function. This two-stage solution algorithm was tested for *constr*, *fminu* and *fmins*. The *fmins* simplex search routine was found to be highly reliable, converging to the same results for a wide range of specified initial actuator positions. This is consistent with the observations of Parkinson and Hutchinson [5] who noted that the Nelder and Mead simplex (NMS) algorithm has proven to be robust, although less efficient than some unconstrained optimization algorithms. A block diagram of the algorithm incorporating *fmins* is shown in figure 5.

The outer stage of the algorithm uses *fmins* to perform a simplex search to determine the actuator positions for fixed voltages. The inner stage of the algorithm uses *fmins* to determine the optimum actuator input voltages for each set of actuator positions evaluated by the outer stage.

## 5. Analytical results

The problem consisted of determining the optimum locations and voltages for actuators on a one meter long cantilever beam to best approximate a desired parabolic beam shape with tip deflection equal to 0.1% of the beam length. The beam was specified to have the properties of 7075-T6 aluminum, a width of 5.08 cm (2.00 in) and a thickness of 1.575 mm (0.062 in). The beam curvature per unit actuator input voltage was calculated for a symmetrically mounted pair of 0.26 mm (10 mm) thick Navy Type II piezoceramic actuators covering 75% of the width of the beam. Each actuator length was fixed at 10% of the overall beam length. The algorithm was tested with at least four sets of arbitrarily selected initial actuator locations for each number of actuators to ensure convergence to the same optimum values. Initial actuator voltages were the optimum voltages for the initial actuator locations for each case, determined using *fmins*, except when noted.

The deflections of the beam are shown in figures 6, 7, 8 and 9, for one, two, three and four actuators, respectively, located at the optimum locations and input voltages to minimize the error between the desired and actual beam deflection.

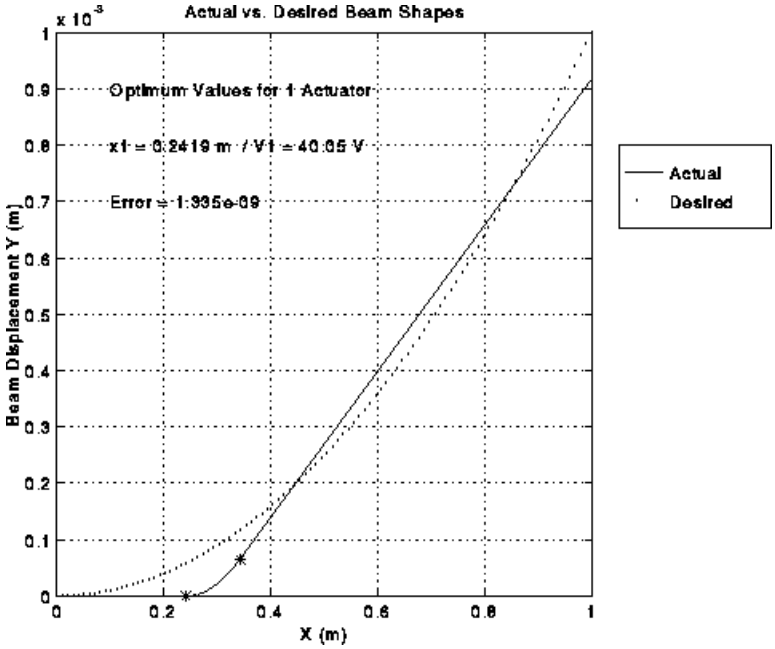


**Figure 6.** Optimum beam deflection for one actuator.

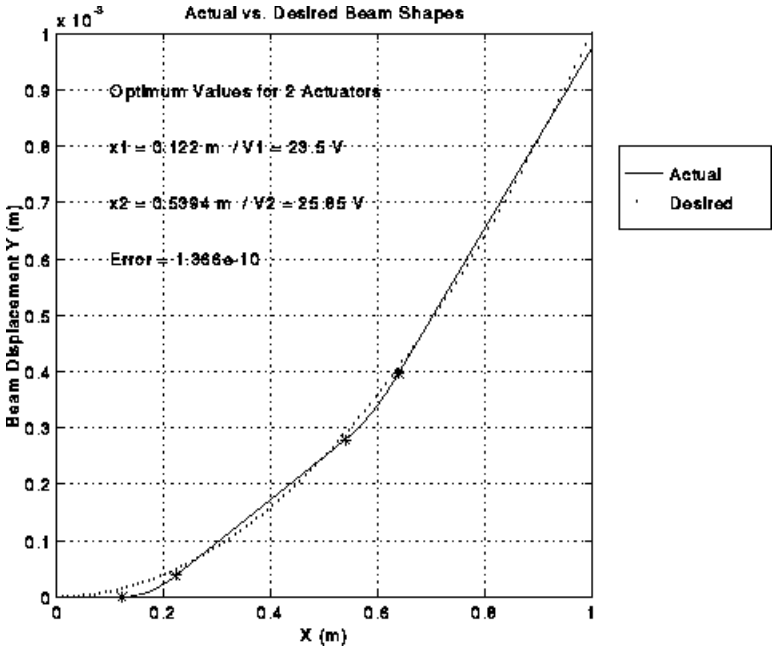


**Figure 7.** Optimum beam deflection for two actuators.

The optimization algorithm proved to have minimal sensitivity to the initial actuator locations specified, with two exceptions. First, grouping the initial locations for four actuators adjacent to one another at the center of the beam, and using optimum voltages for its initial configuration as an initial estimate for all voltages, prevented the inner voltage optimization algorithms from converging within the set of a maximum of 10 000 iterations at some point during the optimization process. Second, using the same actuator locations with initial voltage estimates of zero produced erroneous results. For this case, however, slightly changing the initial condition to allow 1–2% of the beam length spacing between the initial actuator positions produced results consistent with those using other initial conditions.

The results of the actuator voltage optimization algorithm were compared to the exhaustive searches for all possible combinations of discrete sets of actuator voltages for optimum locations of the actuators. Figures 10 and 11 show the plots of the variation of error with the input voltages for one and two actuators, respectively. The results validate the voltage optimization algorithm. The results of the actuator placement optimization algorithm were similarly validated by the search method.

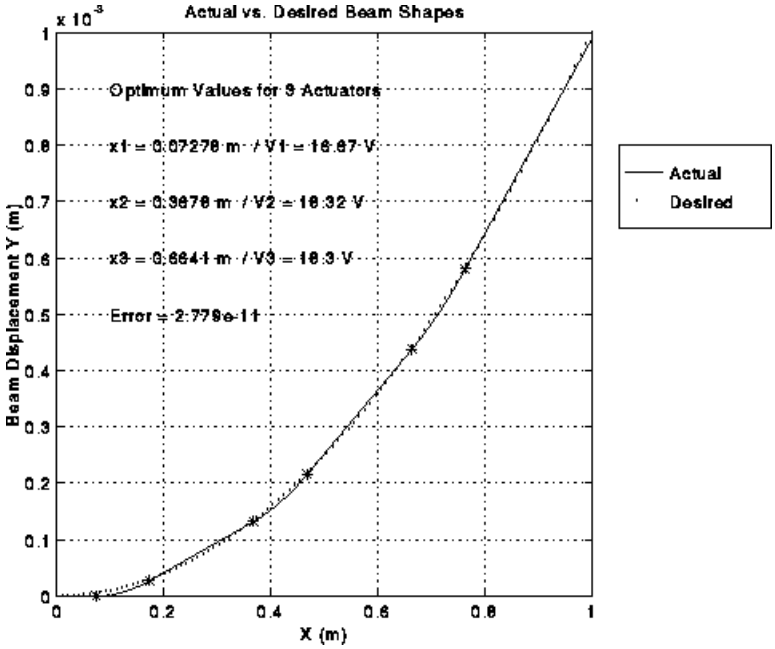


**Figure 8.** Optimum beam deflection for three actuators.

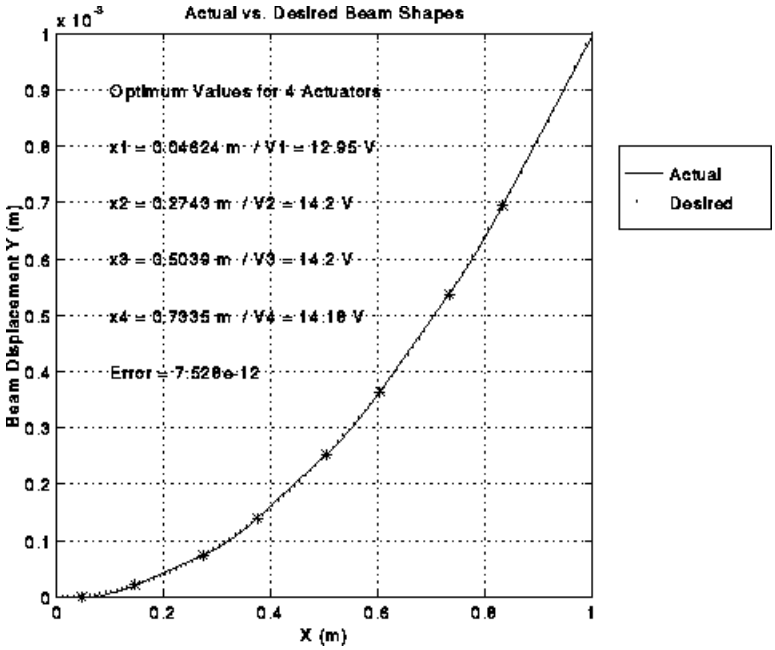


**Figure 9.** Optimum beam deflection for four actuators.

## 6. Experimental results

A schematic of the equipment setup for the four-actuator shape control experiment to determine the effectiveness of piezoelectric actuators for shape control is shown in figure 12 and the setup is pictured in figure 13.

Eight piezoceramic actuator patches were bonded (in four groups of two) to one side of a 0.031 inches (0.79 mm) thick 7-75-T6 aluminum beam which was cantilevered such that its length was horizontal and its width was vertical to allow bending of the beam to take place in the horizontal plane. The beam was supported at approximately two-thirds of its length by an air pad riding on a granite table. The beam had a length of 45 inches (1.143 m), 2 inches (5.08 cm) of which was held in the clamp, and a width of 1.625 inches (4.1275 cm). All actuator patches were 2.5 inches (6.35 cm) long, 1.5 inches (3.81 cm) wide and 0.26 mm thick Navy Type II piezoceramic. The actuators were placed at locations on the beam which were determined by the optimization algorithm to best approximate a parabolic deflected beam shape. The XANALOG system was used to control actuator input and record experimental data, and the ANL1651AC laser displacement was used to measure displacement at selected points along the length of the beam. Beam surface

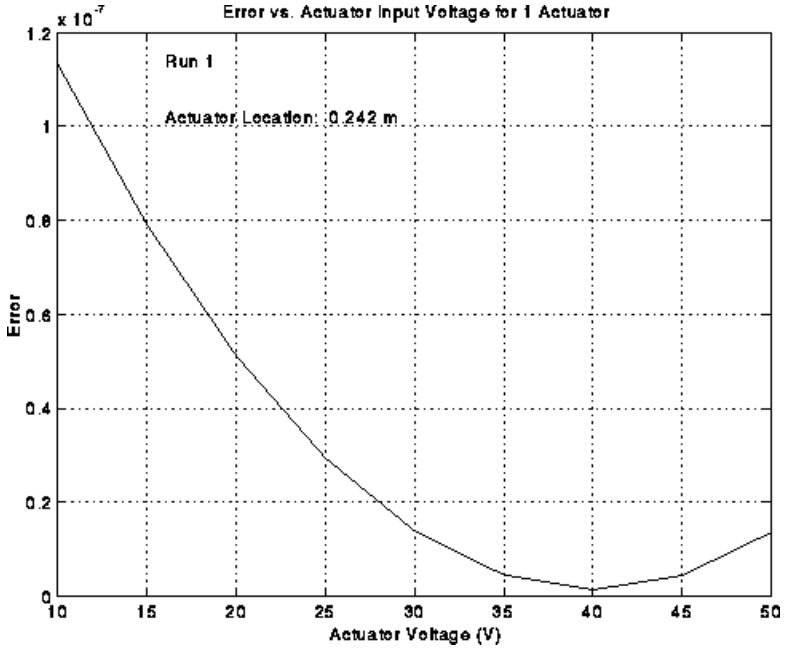


**Figure 10.** Variation of error with input voltages for one actuator at optimum location.

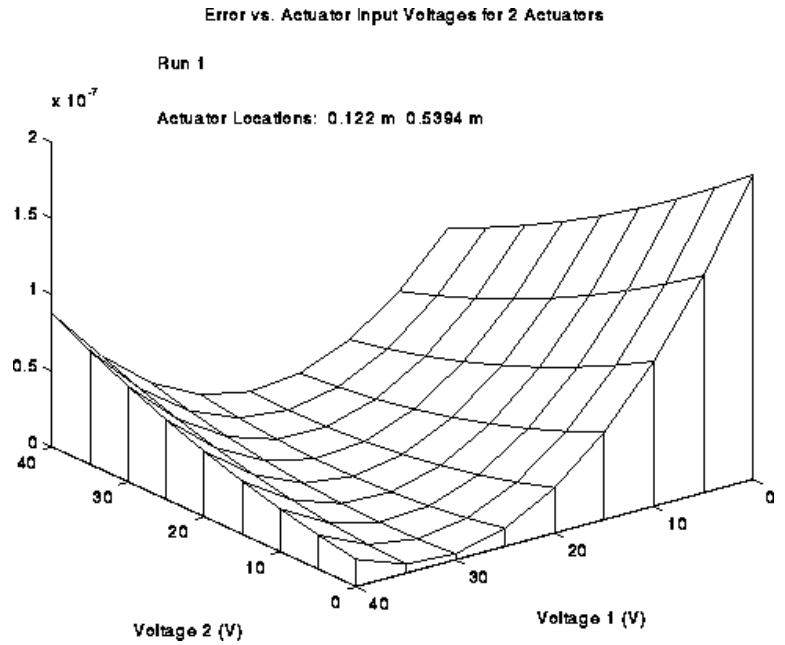


**Figure 11.** Variation of error with input voltages for two actuators at optimum locations.

strain was also measured directly opposite the center of the actuator patch nearer to the cantilevered end of the beam in each of the four actuator groups using a Measurement Group Inc. CEA-13-125WT-350 bi-directional strain gage opposite the other three actuators. Strain gage output was obtained with a Gould Model 56-1301-00 DC/bridge/transducer signal conditioner for each gage. DAS16/330 and DDA06 boards were used for A/D and D/A conversion, respectively. Each 10 volt analog output channel of the DDA06 was amplified by a 15:1 analog amplifier to provide a 150 volt range of input to each actuator.

The first phase of the experiment was to determine the performance of each actuator. Data for beam deflection for the first actuator are presented in table 1 and figure 14.

The first run was the first use of that actuator on the day of the experiment. The deflection reading was initialized at the start of a new run. Some hysteresis and residual displacement were observed on all measurement runs, but were most apparent on the first run with a residual tip displacement of 16%. Repeatability of displacement measurement was good for runs 2 through 4. The relationship between actuator input voltage and beam tip displacements was nonlinear, as seen in figure 14. The dotted line represents a second-order least

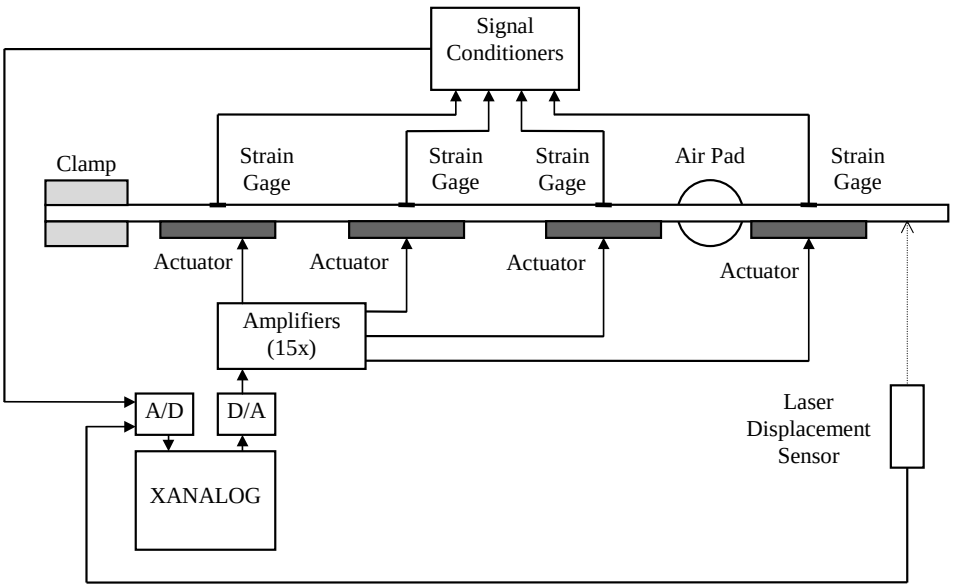


**Figure 12.** Schematic of setup of four-actuator shape control experiment.

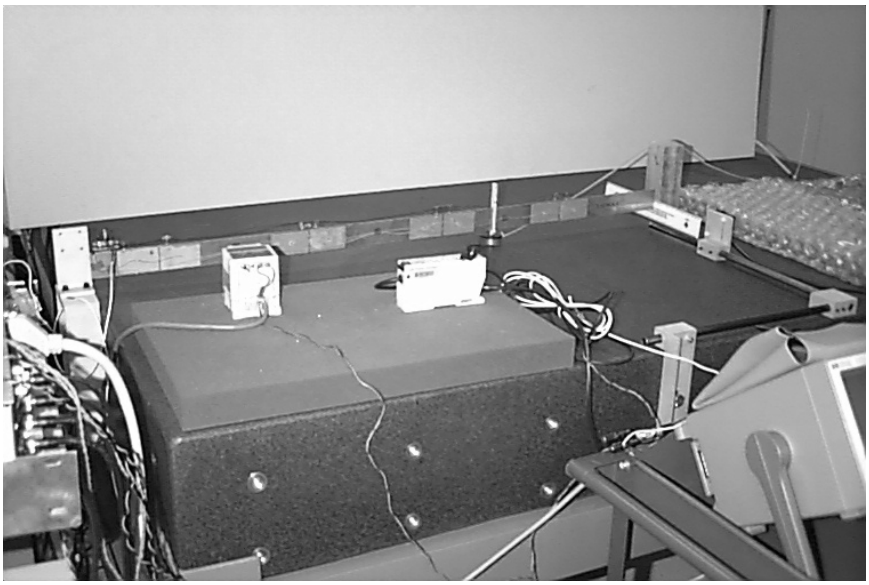

**Figure 13.** Setup of four-actuator shape control experiment.

squares curve fit of the form

$$y_0(V) = c_0 V^2 + c_1 V + c_2 \tag{29}$$

to the observed displacements as a function of voltage. Using a linear model, the predicted value of $c_1$ is $7.92 \times 10^{-2}$ mm V$^{-1}$. Based on the experimental results, the values of coefficients for the non-linear model are: $c_0 = 3.18 \times 10^{-4}$ mm V$^{-2}$, $c_1 = 5.38 \times 10^{-2}$ mm V$^{-1}$ and $c_2 = -0.10$ mm. The performances of the other actuators were very similar.

The second phase of the experiment consisted of applying voltages to all four actuators based on an analytical model, and optimal search routines to minimize the error between desired parabolic shape and predicted deformed shape. Table 2 and figure 15 present applied voltages to actuators, predicted deflections based on the linear model and the empirical nonlinear model, and the experimentally determined deflections.

The measured displacements display excellent repeatability and can be seen to agree much more closely with the beam shape profile predicted using the nonlinear empirical model than for the profile predicted by the linear model. As for the single-actuator tests, the linear model overestimates the actuator performance for the low input voltages and underestimates actuator performance at higher voltages.

## 7. Conclusions

Piezoceramic actuators have been shown to provide an effective means of controlling the shape of a thin flexible

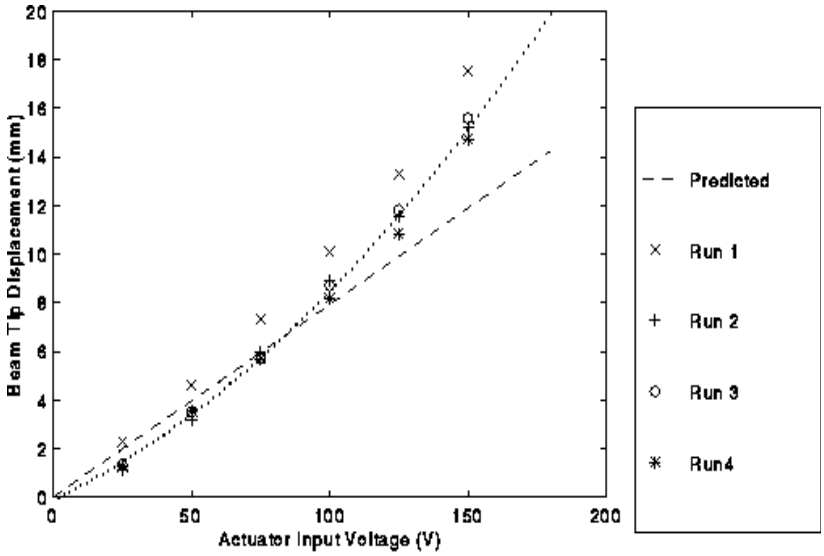


**Figure 14.** Beam tip displacement for first actuator.

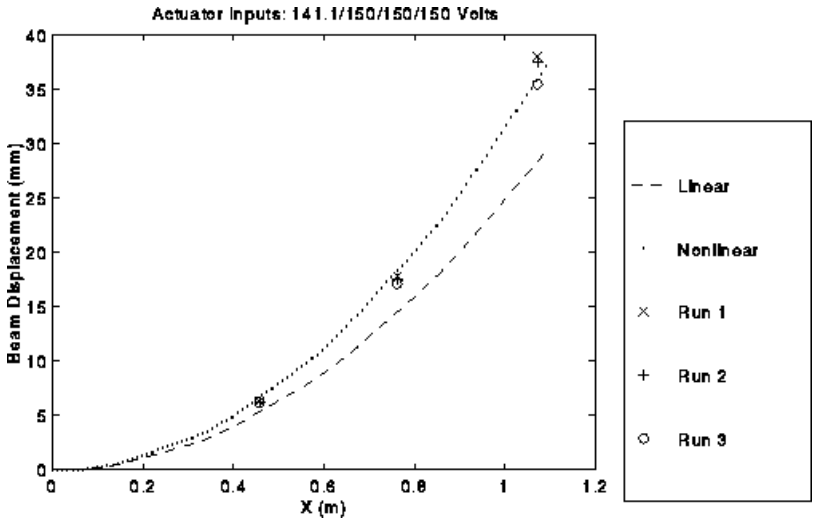


**Figure 15.** Beam displacement measurements for shape control experiment.

**Table 1.** Beam tip displacement (mm (% of predicted)) for first actuator.

| | Predicted | 1 | 2 | 3 | 4 |
|---|---|---|---|---|---|
| 25 V | 1.47 | 1.29 (88) | 1.31 (89) | 1.12 (76) | 1.27 (86) |
| 50 V | 2.93 | 3.06 (104) | 2.71 (93) | 2.67 (91) | 2.76 (94) |
| 75 V | 4.40 | 5.45 (124) | 4.54 (103) | 4.38 (100) | 4.45 (101) |
| 100 V | 5.86 | 8.08 (138) | 6.44 (110) | 6.41 (109) | 6.22 (106) |
| 125 V | 7.33 | 11.22 (153) | 8.88 (121) | 8.47 (116) | 8.81 (120) |
| 150 V | 8.79 | 15.05 (171) | 11.81 (134) | 11.40 (130) | 11.62 (132) |
| 0 V | 0.00 | 3.57 | 0.81 | 0.31 | 0.85 |

beam structure. The location of actuators on a beam structure is crucial to determining how closely a desired deformation profile can be approximated. Simultaneous optimization of the locations and input voltages of a fixed set of actuators to achieve a desired beam deformation proved to be unreliable due to differences in the order of the actuator locations and voltage terms in the optimization cost function. Using embedded Nelder and Mead simplex algorithms to separately optimize actuator locations and input voltages was found to produce much more reliable results, converging to the same optimum solution for a variety of initial conditions. A few initial conditions were found to cause the optimization algorithms to fail to converge or converge to an erroneous result. Therefore, multiple runs of the optimization should be performed using different sets of initial conditions to ensure that globally optimum actuator locations and voltages are obtained. The significant effects of hysteresis observed indicate that this effect must also be considered. Actual

**Table 2.** Beam displacement measurements (mm) for shape control experiment.

| | Linear model predicted | Nonlinear model predicted | Run 1 | Run 2 | Run 3 |
|---|---|---|---|---|---|
| 141.1/150/150/150 V input | | | | | |
| $x = 0.46$ m | 5.30 | 6.65 | 6.23 | 6.16 | 6.17 |
| $x = 0.76$ m | 14.48 | 18.29 | 17.76 | 17.54 | 17.08 |
| $x = 1.07$ m | 28.33 | 35.91 | 37.98 | 37.54 | 35.45 |

shape control applications should incorporate some form of feedback of the beam's shape to ensure that the desired deformation is attained.

## References


[1] Crawley E F and Anderson 1990 Detailed models of the piezoceramic actuation for beams *J. Intell. Mater. Syst. Struct.* **1**

[2] Crawley E F and de Luis J 1987 Use of piezoelectric actuators as elements of intelligent structures *AIAA J.* **25** 1373–85

[3] Clark R L and Fuller C R 1992 Optimal placement of piezoelectric actuators and polyvinylidene fluoride error sensors in active structural acoustic control approaches *J. Acoust. Soc. Am.* **92**

[4] Wang B T, Burdisso R A and Fuller C R 1994 Optimal placement of piezoelectric actuators for active structural acoustic control *J. Intell. Mater. Syst. Struct.* **5**

[5] Parkinson J M and Hutchinson D 1972 A consideration of non-gradient algorithms for the unconstrained optimization of functions of high dimensionality *Numerical Methods for Optimization* ed F A Lootsma (New York: Academic)